

# Structural and Optical Properties of Co-precipitated Mn-doped TiO<sub>2</sub> Nanoparticles

Prasoppon Junlabhut\* and Pilaipon Nuthongkum

*Department of Applied Physics, Faculty of Science and Technology, Rajabhat Rajanagarindra University, Chachoengsao, Thailand*

## Abstract

Mn-doped TiO<sub>2</sub> nanoparticles have been synthesized by conventional co-precipitation process with different dopant concentrations. As-synthesized products were calcined at 400-700°C for 3 h in order to improve their crystallinity. The crystalline phase structure, surface morphology and optical properties of Mn doped TiO<sub>2</sub> nanoparticles were investigated by X-ray diffraction, Scanning electron microscope and UV-Vis spectroscopy. The phase transformation from anatase to rutile occurred when the calcination temperature increases beyond specific temperature. SEM images revealed the agglomerated spherical shapes of the product. XRD results were shown the crystalline sizes of TiO<sub>2</sub> decreased depending on high Mn doping due to the influence of Mn charge and ionic radius incorporated into Ti lattice. The optical spectra of doped products exhibit a noticeable red shift of absorption edge toward visible region. This occurrence may imply the decrease of the optical band gap with increasing Mn doping content.

**Keywords:** Manganese doping, Mn doped TiO<sub>2</sub> nanoparticles, Co-precipitation method.

## 1. Introduction

The Nanocrystalline titanium dioxide has been widely studied in recent years due to its potentially photocatalytic activities, strong absorption in the UV region, good photocatalytic activity, non-toxic, inexpensive, high chemical stability and mechanical stability [1]. TiO<sub>2</sub> is well known as a high potential semiconductor in various applications, for example, environmental purification, filter membrane, solar cell, photoconductor and gas sensor [2]-[4]. However, high electron hole pair recombination rate is the main problem with decreasing TiO<sub>2</sub> efficiency. Meanwhile, wide direct band gap (3.2 eV for anatase phase and 3.02 eV for rutile phase) is also the limitation of light illumination only UV region relating to less exciting in visible light. Therefore, high efficiency of inhibition the electron hole pair recombination becomes necessary of TiO<sub>2</sub> photocatalytic. TiO<sub>2</sub> has three different crystalline phase anatase, rutile and brookite. TiO<sub>2</sub> nanostructures have been recognized as a versatile metal oxide nanostructure for various applications. It depends on their synthesis, structure in term of crystallinity, morphology, and size. However, low absorption in visible region corresponds to only 3-5% of solar radiation and high recombination rate of electron-hole pair are the main drawbacks of TiO<sub>2</sub>. For solving the main drawbacks of TiO<sub>2</sub>, doping with additive material was studied to improve its efficiency. Dopant materials include non-metal such as C, N, and S and transition metal such as Fe, Co, Ni, Cu and Mn can generate an impurity level under conduction band resulting in preventing charge recombination [5-6]. Mn dopant demonstrates the great potential as a guest material in TiO<sub>2</sub>. The optical absorption edge can shift due to effective band tuning by the influence of Mn dopant incorporation [2].

The modification of tunable TiO<sub>2</sub> band gap from metal doping can be successfully prepared in various methods. Mn doped TiO<sub>2</sub> nanoparticles can be synthesized via sol-gel method [3], hydrothermal process [7], and co-precipitation process [8]. Comparing with other process, the advantages of co-precipitation process can be described as low cost, ease of doping, short processing time and large capability to produce homogenous particles and multi-component metal oxide [9].

Recent research works have been reported on structural and optical properties of co-precipitated Mn doped TiO<sub>2</sub> nanoparticles. The samples of Un-doped and Mn doped TiO<sub>2</sub> nanoparticles were synthesized by co-precipitation method with varying Mn dopant concentrations. The nanocrystalline phase structure, surface morphology and optical properties of un-doped and Mn doped TiO<sub>2</sub> nanoparticles were investigated by X-ray diffraction, scanning electron microscope and UV-vis spectroscopy

## 2. Procedure

Mn doped TiO<sub>2</sub> nanoparticles were synthesized via co-precipitation method. The amount of Mn dopant concentration was varied in the range of 0-5 mol%. Titanium tetra-isopropoxide [Ti(OC<sub>3</sub>H<sub>7</sub>)<sub>4</sub>] and manganese (II) nitrate tetrahydrate Mn(NO<sub>3</sub>)<sub>2</sub>·4H<sub>2</sub>O were used as starting precursors for Ti and Mn source, respectively. A specific amount of Mn and Ti depending on the desired composition of Mn doping was dissolved in absolute ethanol under vigorous stirring at room temperature. The colloidal solution was successfully stirred for 30 min until a clear and transparent solution to obtain the adsorption equilibrium. During this phase an exchange of Mn with Ti occurs and the solution was mixed. After that, the remaining Ti ions were forced to co-precipitation by adding the precipitated agent (NH<sub>4</sub>OH) in mixed solution slowly drop until pH 9 [3-4]. The solution was stirred continuously at room temperature for 3 h followed by aging at room temperature for 24 h. After aging process, as-prepared precipitates were filtered and washed several times with DI water to remove residue and impurities until pH became neutral. As-synthesized un-doped and Mn doped TiO<sub>2</sub> products were dried in oven at 100°C for 24 h. Finally, un-doped and Mn doped TiO<sub>2</sub> nanopowders with various Mn dopant concentrations was calcined at 400-800 °C for 3 h. Nanocrystalline structure and phase formation of un-doped and Mn doped TiO<sub>2</sub> nanoparticles were characterized by X-ray diffraction (XRD; PANalytical X'Pert Pro) at 40 kV and 30 mA is using Cu-K radiation in the range of 20-80° with a scanning rate of 0.02° s<sup>-1</sup>. The surface morphologies and the elemental compositions of Mn dopant into TiO<sub>2</sub> were monitored by scanning electron microscope (SEM; EVO MA10). Their absorption optical properties were investigated by UV-Vis spectrophotometer with a wavelength range of 200-800 nm.

**Table 1.** Optical bandgap and calculated crystallite size of Mn doped TiO<sub>2</sub> catalyst with various Mn dopant concentrations calculated by Scherrer's equation.

Samples	Un-doped	0.1%Mn doped	0.5%Mn doped	5% Mn doped
Crystalline size (nm)	17.45	13.85	13.44	13.24
Optical bandgap (eV)	3.25	2.95	2.70	3.18

### 3. Results and Discussion

The XRD patterns of Mn doped TiO<sub>2</sub> nanoparticles with various Mn dopant concentrations with calcination at 500 °C for 3 h are shown in Fig. 1. The diffraction peaks of un-doped products show phase information about the pure tetragonal structure of TiO<sub>2</sub> anatase phase. The anatase phase located at 25.3°, 38.0°, 48.2° corresponding (101), (004) and (200) plane, respectively. For Mn doped TiO<sub>2</sub> nanoparticles, there was no trace of phase corresponding to metallic Mn or Mn compound in XRD pattern. The intensity of a diffraction peak with (101) plane tends to decrease with increasing Mn dopant. The peak width of the (101) plane are broadened and slightly shift towards the low angle side indicating well incorporation of Mn ion in lattice of TiO<sub>2</sub> [5], [11]. The crystallite size (D) of the samples estimates by FWHM and peak angle of (101) plane have been calculated using Debye-Scherrer's equation as shown in Table 1..

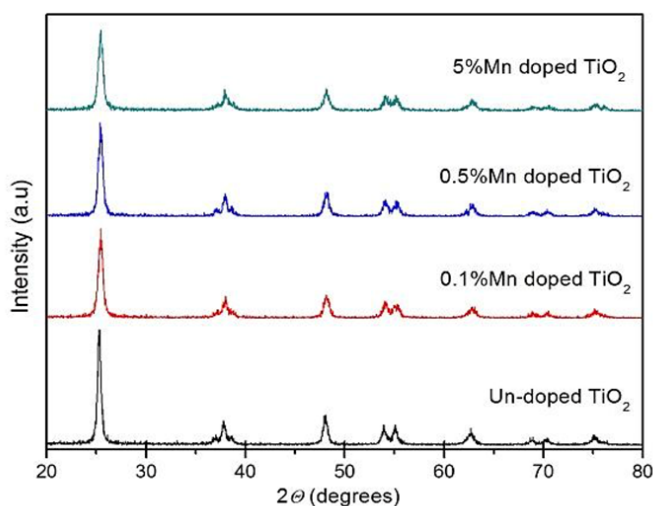


**Fig. 1.** XRD patterns of Mn doped TiO<sub>2</sub> nanoparticles with different Mn dopant concentrations calcined at 500 °C for 3h.

The crystalline sizes of TiO<sub>2</sub> decreased depending on high Mn doping due to the influence of Mn charge and ionic radius. Since Mn can be present in different oxidation states like Mn<sup>2+</sup> (0.80 Å), Mn<sup>3+</sup> (0.66 Å) or Mn<sup>4+</sup> (0.60 Å), the interstitial incorporation of the dopant into titanium structure can be possible. Mn<sup>3+</sup> and Mn<sup>4+</sup> could be placed in the interstitial site due to lower cation than Ti<sup>4+</sup>. It is impossible for incorporation of Mn ions into TiO<sub>2</sub> lattice preserving the anatase phase [12]. The XRD results of 0.5% Mn-doped TiO<sub>2</sub> nano-particles with various calcination temperatures for 3 h are illustrated in Fig. 2. As-synthesized of 0.5% Mn-doped TiO<sub>2</sub> nanopowders was largely amorphous, while the samples at calcine at 300-500 °C indicate that the peak intensity of anatase phase (101) greatly increased with the clear appearance of anatase structure of TiO<sub>2</sub>. One can see that among the nanoparticles calcined at 700 °C, the samples are mixed phase of anatase and rutile. These results indicated that the improvement of TiO<sub>2</sub> crystalline was obtained by the optimizations of calcination temperatures

The morphology of un-doped and Mn doped TiO<sub>2</sub> nanoparticles calcined at 500°C for 3 h was monitored by SEM image as depicted in Fig. 3. All samples were highly dispersed and

homogenized spherical particles. The elemental analysis of 1% Mn doped  $\text{TiO}_2$  analyzed by energy dispersive X-ray analyses (EDX) is shown in Fig. 4. The elemental compositions of the presence of Ti, O and Mn according to weight% and atomic% stoichiometries are listed in Table 2.

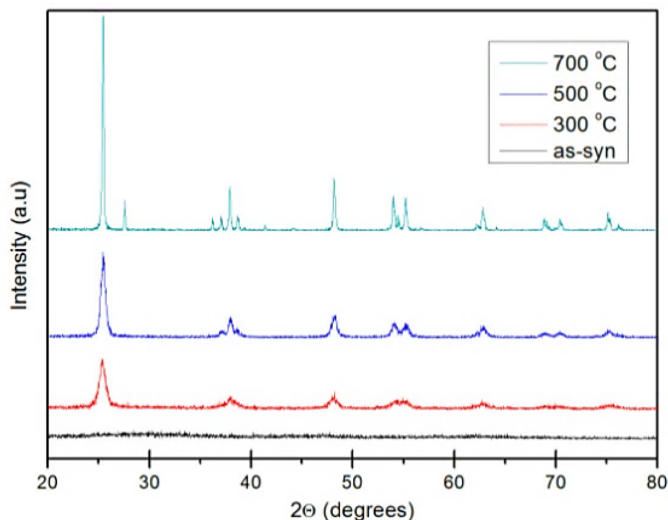


**Fig. 2.** XRD patterns of 0.5% Mn doped  $\text{TiO}_2$  nanoparticles with various calcination temperatures

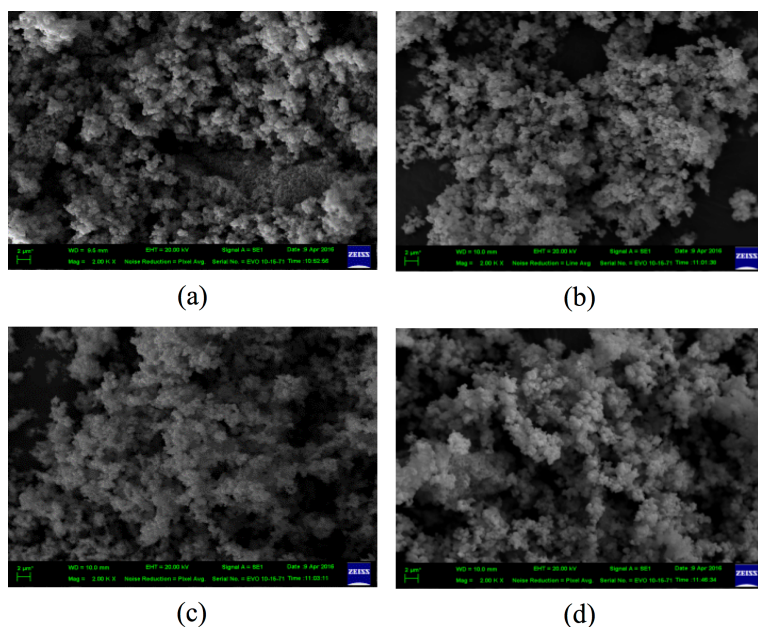


**Fig. 3.** SEM images of un-doped and Mn doped  $\text{TiO}_2$  nanoparticles with various Mn dopant concentrations (a) Un-doped  $\text{TiO}_2$ , (b) 0.5% Mn doped  $\text{TiO}_2$ , (c) 1% Mn doped  $\text{TiO}_2$  and (d) 5% Mn doped  $\text{TiO}_2$  calcined at 500 °C for 3h.

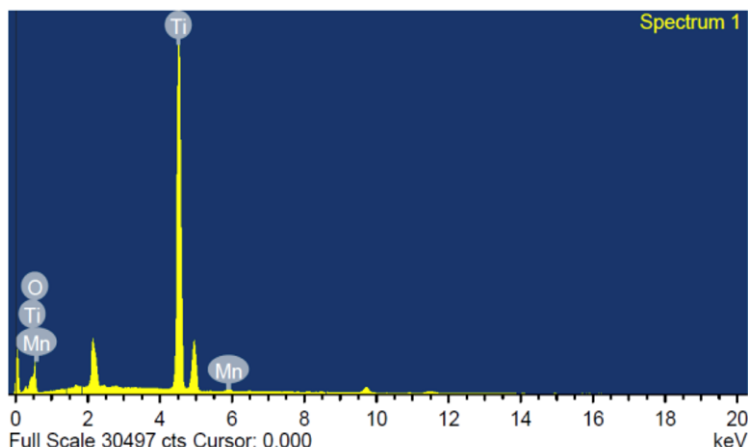


**Fig. 4.** EDX spectra of 1% Mn doped TiO<sub>2</sub> nanoparticles with the calcined temperature at 500 °C for 3h.

**Table. 2.** Elemental composition estimated by EDX analysis with 1% Mn doped TiO<sub>2</sub> with the calcined temperature at 500 °C for 3 h.

Element	Weight %	Atomic %
O K	30.14	56.40
Ti K	69.02	43.14
Mn K	0.84	0.46
Total	100	

The optical absorption spectra of Mn doped TiO<sub>2</sub> nanoparticles are presented in Fig. 5. In the region of 200-800 nm, the absorption increased up to 0.5% Mn doping content, and reduced in 1% Mn dopant. The intensive absorption exhibit slightly increased red shift of absorption edge toward visible region due to the appearance of the electronic states of the Mn doped TiO<sub>2</sub> band gap. The band gaps of pure TiO<sub>2</sub> and Mn doped TiO<sub>2</sub> nanoparticles were determined by Manificier model [2]. The direct band gap energy was evaluated between  $(\alpha hv)^2$  and photon energy ( $hv$ ) by using the equation

$$\alpha hv = A(hv - E_g)^n \quad (1)$$

where,  $hv$  is a photon energy,  $\alpha$  is the absorption coefficient ( $\alpha = 4\pi k/\lambda$ ,  $k$  is absorbance,  $\lambda$  is the wavelength of absorption measurement in nm).  $E_g$  is energy band gap,  $A$  is a constant and  $n = 1/2$  for direct or  $n = 2$  for indirect allowed transition semiconductors. The energy band gap was determined by extrapolating the straight line portion of  $(\alpha hv)^2$  on  $hv$  axis. As shown in Fig. 6, the approximation of the direct band gap energy of un-doped and Mn doped TiO<sub>2</sub> nanoparticles decreases from 3.10 eV to 2.70 eV with 0.5% Mn doping with calcined at 500°C for 3 h. The intense absorption in the visible region is attributed to the

charge transfer interaction between Mn dopant on Ti ions. The decrease of band gap energy with increasing Mn dopant may be a reason for high photoactivity in longer wavelength.

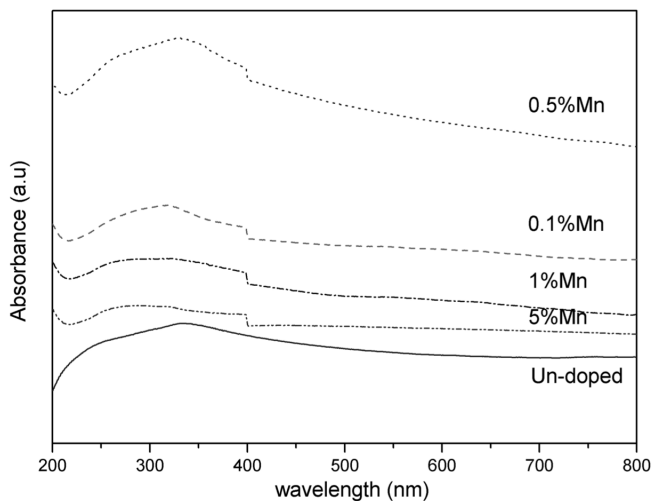


**Fig. 5.** Optical absorption spectra of un-doped and Mn doped TiO<sub>2</sub> nanoparticles with various Mn dopant concentrations calcined at 500 °C for 3h.

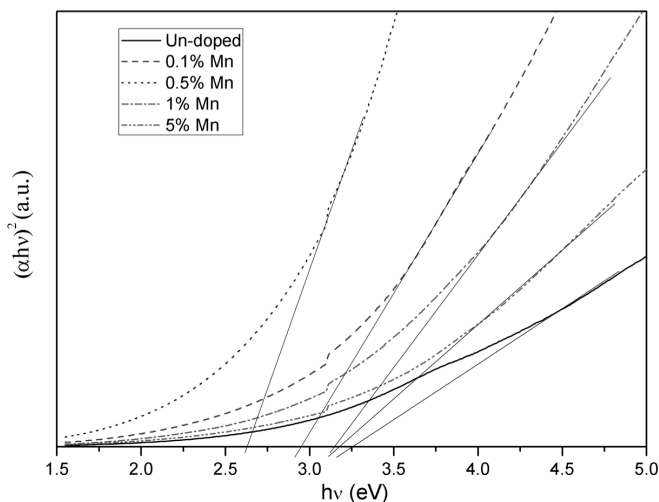


**Fig. 6.**  $(\alpha hv)^2$  versus photon energy ( $h\nu$ ) of Mn doped TiO<sub>2</sub> nanoparticles with various Mn dopant concentrations calcined at 500 °C for 3h.

#### 4. Conclusion

In summary, undoped TiO<sub>2</sub> and Mn doped TiO<sub>2</sub> nanoparticles were successfully synthesized via conventional co-precipitation process with different Mn dopant concentrations. The crystalline sizes of TiO<sub>2</sub> were decreasing about 17 to 13 nm by the amount of Mn doping. The crystalline sizes of TiO<sub>2</sub> increased depending on high Mn

doping due to the influence of Mn charge and ionic radius. It is impossible for incorporation of Mn ions into TiO<sub>2</sub> lattice preserving the anatase phase. The mixture phase of anatase and rutile can be seen as the calcination temperature is higher than 500°C. The morphology of un-doped and Mn doped TiO<sub>2</sub> nanoparticles illustrated highly dispersed spherical particles. The intensive absorption spectra of Mn doped TiO<sub>2</sub> exhibit slightly increased red shift of absorption edge toward visible region due to the appearance of the electronic states of the Mn dopant. The approximation of the direct band gap energy of un-doped and Mn doped TiO<sub>2</sub> nanoparticles decreased from 3.25 eV to 2.70 eV with 0.5% Mn doping using Manificier model. The overall characterization results indicated that the crystalline and optical properties of TiO<sub>2</sub> nanoparticles were significantly affected by Mn dopant.

## Acknowledgements

This work was financially supported by Rajabhat Rajanagarindra University (RRU) for research fund support. This work has partially been supported by the College of Nanotechnology (KMITL). Authors would like to thank faculty of engineering, Rajamangala University of Technology Thanyaburi (RMUTT) for X-ray diffraction measurement and Suan Dusit University for UV-vis measurement.

## References

- [1] L. Samet, J. Ben Nasseur, R. Chtourou, K. March and O. Stephan. *Materials Characterization* 85 (2013), 1-12.
- [2] R. Chauhan, A. Kumar and R.P. Chaudhary. *Spectrochimica Acta Part A: Molecular and Biomolecular Spectroscopy* 98 (2012), 256-264.
- [3] V.D. Binas, K. Sombani, T. Maggos, A. Katsanaki and G. Kiriakidis. *Applied Catalysis B: Environmental* 113-114 (2012), 79-86.
- [4] V.C. Papadimitriou, V.G. Stefanopoulos, M.N. Romanias, P. Papagiannakopoulos, K. Sambani, V. Tudose and G. Kiriakidis. *Thin Solid Films* S20 (2011), 1195-1201.
- [5] Y.F. Zhao, C. Li, S. Lu, R.X. Liu, J.Y. Hu, Y.Y. Gong and L.Y. Niu. *Journal of Solid State Chemistry* 235 (2016), 160-168.
- [6] G.S. Mital and T. Manoj, *Science Bulletin* 56 (2011), 1639-1657.
- [7] X. Xue, W. Ji, Z. Mao, Z. Li, W. Ruan, B. Zhao and J.R. Lombardi. *Spectrochimica Acta Part A: Molecular and Biomolecular Spectroscopy* 95 (2012), 213-217.
- [8] G. Kiriakidis. *Journal of the Korean Physical Society* 65 No. 3 (2014), 1-6.
- [9] P. Junlabhut, C. Wattanawikkam, W. Phoohinkong, W. Mekprasart, W. Pecharapa, *Key Engineering Materials* 675-676 (2016), 97-100.
- [10] D. Peng, L. Fa-Min, Z. Chuang-Cang, Z. Wen-Wu, Z. Huan, C. Lu-Gang and Z. Le-Gui. *Chinese Physics B*. 19 No. 11 (2010), 1188102.
- [11] S. Paul and A. Choudhury. *International Journal of Innovative Research and Development* 1 issue 7 (2012), 24-31.
- [12] A. Perez-Larios, A. Hernandez-Gordillo, G. Morales-Mendoza, L. Lartundo-Rojas, A. Mantilla and R. Gomez. *Catalysis Today* 266 (2016), 9-16.